Front. Earth Sci. 2025, 19(1): 135−148
https://doi.org/10.1007/s11707-022-0981-6

RESEARCH ARTICLE

Paleoenvironmental changes and East Asian winter monsoon evolution: evidence from coastal sedimentary sequence of the Last Glacial in the Shandong Peninsula, China

Zhiwen LI[1,2,3], Fengnian WANG (✉)[4], Baosheng LI[5], Dingding DU[2], Huijuan ZHANG[2], Yougui SONG[3], Shuhuan DU[6], Li SUN[1]

1 School of Environmental and Chemical Engineering, Foshan University, Foshan 52800, China
2 State Key Laboratory of Nuclear Resources and Environment, East China University of Technology, Nanchang 330013, China
3 State Key Laboratory of Loess and Quaternary Geology, Institute of Earth Environment, Chinese Academy of Sciences, Xi'an 710061, China
4 School of Geography and Tourism, Huizhou University, Huizhou 516007, China
5 School of Geography, South China Normal University, Guangzhou 510631, China
6 Key Laboratory of Marginal Sea Geology, South China Sea Institute of Oceanology, Chinese Academy of Sciences, Guangzhou 510301, China

Abstract The coastal sediments are sensitive carriers that reveal climate change, sea-level fluctuations, and monsoon evolution. A large number of sedimentary sequences developed along the coast of the Shandong Peninsula in the Last Glacial Period. Previous studies mainly focused on material sources and climate characteristics, but seldom mention the ten-thousand-year timescale monsoon evolution and its relationship with sea level fluctuations. The Liukuang section (LKS) is adjacent to the North Yellow Sea, which is mainly composed of alternations of dune sand and paleosol of the Last Glacial. Based on the chronological framework constructed by AMS ^{14}C and optically stimulated luminescence (OSL) dating, we measured grain size, geochemistry, and heavy minerals to reconstruct the evolution of the East Asian winter monsoon (EAWM) and climatic fluctuations during the Last Glacial Period. The variations of the climate proxy indicators show that the degree of dry-cold climate and EAWM strength are indicated by different sedimentary facies in dune sand > sandy paleosol > lacustrine > silty paleosol. On a ten-thousand-year timescale, we detected episodes of EAWM strengthened in the LKS4 (78.9— 59.5 ka), LKS3b (50.5— 39.6 ka) and LKS2 (29.7— 13.1 ka), which correspond to Marine Isotope stage (MIS) MIS4, MIS3b and MIS2, respectively, and EAWM weakened in the LKS3c (59.5— 50.5 ka) and LKS3a (39.6— 29.7 ka), which correspond to MIS3c and MIS3a, respectively. These climatic events were essentially synchronous with climate changes recorded in the geological carriers such as the cave stalagmites of southern China, loess from the Chinese Loess Plateau (CLP), and sea-level fluctuations in the Yellow-Bohai Sea. It is believed that the external driving factor is from the changes of solar radiation, and the internal factor is mainly from the combined effect of monsoon changes and sea-level fluctuations.

Keywords aeolian sand deposition, last Glacial Period, East Asian monsoon evolution, sea-level fluctuation, Shandong Peninsula

Received September 6, 2021; accepted March 3, 2022

E-mail: 407890145@qq.com

1 Introduction

Various geological medium are used to reveal the climatic characteristics of the Last Glacial Period, including Greenland ice cores (Stuiver and Grootes, 2000), deep-sea sediments (Heinrich, 1988), stalagmites (Wang et al., 2001, 2008; Cheng et al., 2016), and Chinese loess (Porter and An, 1995; An et al., 1991, 2015). The medium can record the ten-thousand-year events of the warm Marine Isotope Stage 3 (MIS3) interstadial and two cold stadials (MIS4 and MIS2), together with the millennial-scale climatic fluctuations termed extremely cold Heinrich (H) events.

The coastal zone, subject to the intersection of continent and ocean, has experienced frequent and intense ocean-land-atmosphere interactions. Its Quaternary

geological processes are characterized by erosion, sediment accumulation and weathering under the combined effects of climate and sea level change. Climate change affects the strength of aeolian sand activity and weathering degree, and sea-level fluctuations affect the provenance supply and transport distance of aeolian sand activities. Therefore, coastal aeolian sand deposition can provide abundant information about climatic change and sea-level fluctuations. Based on the sedimentary facies and their physical and chemical properties of coastal zone sediments, the climate change and sea-level fluctuations have been widely studied on a ten-thousand-year timescale (Zazo et al., 2008; Andreucci et al., 2009; Fornós et al., 2009; Du et al., 2014, 2016; Li et al., 2019).

The sedimentary deposits along the northern coast of Shandong Peninsula, bordering the north Yellow Sea, are the important medium for studying climate change, sea-level fluctuations, and monsoon evolution in this region. The history of Pleistocene climatic change and sea-level fluctuations has been reconstructed from the sediments of the Yellow Sea and the Bohai Sea (IOCAS, 1985; Yi et al., 2012, 2017). In addition, sediment sources and climatic change have been investigated in studies of coastal loess and paleosol (Cao et al., 1988; Du et al., 2014, 2016; Li et al., 2019). However, there only a few studies about aeolian sand system of the "Liukuang red bed" during the Last Glacial Period (Zhang and Liu, 1992; Guo and Li, 1994). Notably, in the study area, the Last Glacial was characterized by frequent climatic changes and high-magnitude sea-level fluctuations. Consequently, it is of great significance to clarify the regional depositional characteristics, climatic fluctuations, and their driving factors on ten-thousand-year timescale which are still unclear.

Based on several investigations of the Bohai Sea and North Yellow Sea coastal zone, we present the Liukuang stratigraphic section (LKS) on the edge of the North Yellow Sea, which is composed of aeolian sand, sandy paleosol, silty palesol, and lacustrine facies. We constructed the chronological framework using AMS ^{14}C and OSL dating ages, and then measured grain size, chemical elements, and heavy mineral. The description and interpretation of this work yields insight to reveal the governing changes of the aeolian sand environment in the coastal zone, and its relationship with regional and global climate change, including the changes of EAWM intensity and sea-level fluctuations.

2 Geological background

2.1 Geological and geographical overview

The LKS is located in Rongcheng City, in the northern coastal zone of Shandong Peninsula, China. It is located in the eastern part of the modern monsoon zone, belonging to the warm temperate zone. It is a transition zone from the subtropical zone in the middle-low latitudes to the temperate zone in the middle-high latitudes. Meanwhile, it is a typical area where EAWM and EASM alternately prevail, and is also affected by prevailing westerly wind (Gao, 1962). Therefore, the northern coast of Shandong Peninsula is an important belt for heat and moisture transportation between the subtropical and temperate zones.

Geographically, the study area lies between the eastern part of the Eurasian continent and the western margin of the Pacific Ocean, and has suffered intense ocean-land-atmosphere interactions. The adjacent Bohai Sea is an inland sea with an average water depth of 33 m, and the Yellow Sea is a marginal sea with the continental shelf sloping gently from north-west to south-east and gradually transitioning to the North Pacific. Due to the shallow water and large sea-level fluctuations during the Last Glacial Period, a series of transgression-regression events led to continuous changes of transport-deposition center, which had an important impact on the sediments of the Last Glacial near the present coastal zone, resulting in several sedimentary cycles composed of aeolian sands and paleosols or lacustrine facies.

Rongcheng City, where the section is located, lies at the eastern end of the Jiaobei Uplift of the Jiaodong Shield, on the south-eastern part of the Rushan-Weihai compound anticline, where magmatic rocks are well developed and widely exposed. Long-term weathering and erosion have created a landform type dominated by mountains, hills, and plains, and there are numerous flat-topped hills and shallow valleys with an average elevation of 25 m. The coastline is mostly rocky with the hills penetrating into the Yellow sea to form a steep cape and the valley forming a bay. There are many accumulations of slope, alluvial, and aeolian deposits in the bays.

The area has a warm monsoon humid climate with a continental index of 53.1, with clear four seasonal and monsoonal changes. The multi-year average temperature is 11.3°C, the average temperature of the coldest month is −2.7°C in January, and that of the warmest month is 24.3°C in August. The multi-year average rainfall is 785 mm, and on average 72% of the rainfall falls during June and September. The multi-year average wind speed is 3.1 m/s, and the maximum wind speed is 19 m/s.

The vegetation is warm-temperate deciduous broad-leaved forest, which is mainly composed of arbor forests dominated by *Pinus densiflora*, *Robinia pseudoacacia*, *Pinus thunbergii*, and *Quercus* spp., the shrub forest is dominated by *Quercus acutissima* scrub, and herbaceous plants dominated by *Eriophorum* and *Sanguisorba officinalis*. The soil is mostly composed of granite and its weathered material, its texture is relatively coarse and mainly brown to coarse brown soil, and it is mainly aeolian sandy soil in the coastal area (Local History

Compilation Committee of Rongcheng in Shandong Province, 1999).

2.2 Stratigraphy of the Liukuang section

The LKS (37°24′N and 122°34′E, ~15 m a.s.l.) is located in a cape-bay area formed by a granite mountain. The section is ~100 m from the modern coastline where modern aeolian sand deposits are widely distributed, and consists of 27 strata from the top to bottom. The strata LK1−LK6 belong to the Holocene and are mainly composed of modern aeolian sand, sandy paleosol, and reticulated paleosol. Strata LK7−LK19 belong to the Last Glacial Period and are mainly composed of dune sand and sandy paleosol. The strata LK20−LK24 belong to the Last Interglacial Period and are mainly composed of lacustrine sediments and reticulated paleosols.

In this paper, we focus on the Last Glacial Period, within the depth interval of 588−239 cm, which includes seven layers of dune sand (total thickness of 246 cm, the morphological features of LK7 is shown in Fig. 1(a)), five paleosol layers (total thickness of 68 cm, the morphological features of LK16 is shown in Fig. 1(b)), and two layers of lacustrine sediments (total thickness of 36 cm). All 175 samples were collected at 2-cm intervals. The stratigraphical sequence is shown in Table 1.

3 Materials and methods

3.1 Dating method

A sample was collected for AMS ^{14}C dating of total organic matter, sample preparation and analysis were conducted at the radiocarbon sample preparation laboratory of the Guangzhou Institute of Geochemistry, Chinese Academy of Sciences (CAS), and the State Key Laboratory of Nuclear Physics and Nuclear Technology, Peking University. In addition, eight samples were collected for OSL dating, which was conducted at the Groundwater, Mineral Water and Environmental Monitoring Center of the Ministry of Land and Resources of China. Measurements

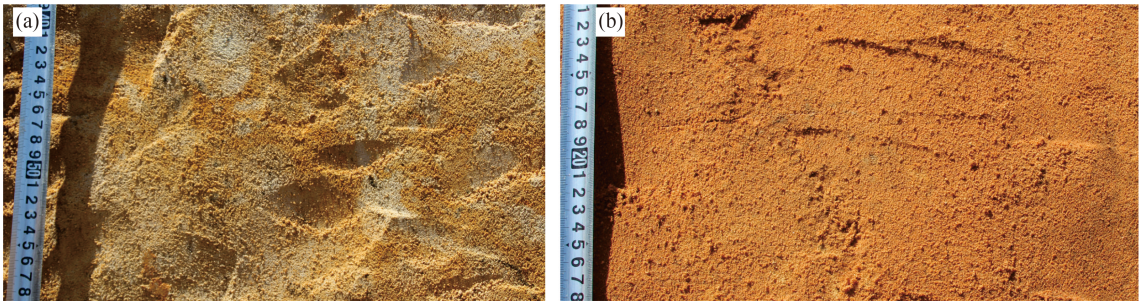

Fig. 1 Main sedimentary facies in Last Glacial Period in the LKS: (a) dune sand; (b) sandy paleosol.

Table 1 Sedimentary facies of the Last Glacial period within the LKS

Horizon	Sedimentary facies	Stratigraphical description	Dating sample
LK6	Reticulated paleosol		1 ^{14}C sample
LK7 (239−278 cm)	Dune sand	Orange yellow-light to brownish red, slightly cemented, no bedding, with humus spots, occasionally off-white spots or stripes < 1 cm	1 OSL sample
LK8 (279−296 cm)	Lacustrine	Gray black-black, with more humus, with off-white and orange yellow patches	
LK9 (297−316 cm)	Dune sand	Yellow-orange yellow, no bedding, slightly cemented	1 OSL sample
LK10 (317−334 cm)	Silty paleosol	Yellow red-light red, relatively compact, with a few carbon spots and off-white stripes	
LK11 (335−374 cm)	Dune sand	Dark grayish yellow, slightly cemented, no bedding, with more carbon spots	1 OSL sample
LK12 (375−384 cm)	Sandy paleosol	Dark brownish red, medium cementation, no bedding, with more carbon spots	
LK13 (385−412 cm)	Dune sand	Yellow-red, slightly cemented, no bedding, partially visible carbonaceous spots	1 OSL sample
LK14 (413−424 cm)	Sandy paleosol	Bright brownish red, slightly cemented, no bedding, carbon spots can be seen locally	
LK15 (425−468 cm)	Dune sand	Grayish white, loose, no bedding	1 OSL sample
LK16 (469−504 cm)	Upper lacustrine/lower paleosol	Upper part is blue gray, no obvious bedding, and contains more carbon and rust spots.Lower part is light brown, compact, and contains more carbon spots	
LK17 (505−532 cm)	Dune sand	Grayish white-grayish yellow, loose with no bedding	2 OSL samples
LK18 (533−542 cm)	Sandy paleosol	Grayish brown, slightly compact	
LK19 (543−590 cm)	Dune sand	Yellowish red to brownish red, slightly cemented, no bedding, with a small amount of carbon spots	1 OSL samples

were made with an American Daybreak 2200 OSL analyzer. Quartz particles in size of 8−15 μm were selected and the equivalent dose values were obtained by a simple multi-slice regeneration (SMAR) method.

3.2 Grain-size analysis

Grain-size analysis was conducted at the Sedimentological Laboratory of the School of Geography, South China Normal University, using the Mastersizer 2000M laser grain size analyzer, with a measurement range of 0.02−2000 μm. Sample pretreatment was carefully followed the methods of Konert and Vandenberghe (1997). The procedure was as follows: HCl was added to air-dried samples to remove carbonate, excess H_2O_2 was then added to remove organic matter, followed by 10 mL of $(NaPO_3)_6$ dispersant with a concentration of 0.05 mol/L. After standing for 24 h, the supernatant was removed and the sample was diluted to an appropriate concentration. Further disaggregation was conducted with an ultrasonic cleaner for 1 min before measurement.

The grain sizes were divided into 101 grades: 2−0.10 mm refers to the decimal system, and sizes of <0.10 mm refer to the general classification principle of Chinese loess (Liu, 1985). Grain-size sub-populations are clay (<5 μm), fine silt (5−10 μm), coarse silt (10−50 μm), very fine sand (50−100 μm), fine sand (100−250 μm), medium sand (250−500 μm), and coarse sand (500−1000 μm). The mean grain size (Mz) was calculated based on the formula of Folk and Ward (1957): Mz = (Φ16 + Φ50 + Φ84)/3, and SC/D = [(silt(%) + clay(%))]/sand(%) was also calculated (Li et al., 1991). Mz reflects the average condition of the sediment grain size, which can indicate the transport intensity, the drought degree in source area and transport distance (An et al., 1991; Ding et al., 1996). Its variations not only reflect the pedogenesis of EASM, but also reflect the dust influx rate and dust-bearing strength of EAWM (An and Porter, 1997). Its high value represents weak transport intensity and long transport distance, indicating a warm-humid sedimentary environment, and low value represents strong transport effect and short transport distance, indicating a cold-dry sedimentary environment (Liu et al., 1985; An and Porter, 1997). The SC/D ratio enlarged the proportional relationship of grain size >4.32Φ and <4.32Φ, which illustrates the two different wind direction alternating and strength change in the East Asian monsoon system (Li et al., 1991). Its low value (<1) indicates sand sediment under the strong wind by dry-cold climate, and a high-value (>1) indicating a weakened or ceased sand activities in the warm-humid climate and enhanced weathering pedogenesis (Li et al., 1991).

3.3 Geochemistry analysis

Thirty-six samples were selected at 10 cm intervals for analysis of chemical elements by the Cold and Arid Regions Environmental and Engineering Research Institute, CAS. The instrument was an Axios sequential wavelength dispersion X-ray fluorescence spectrometer (PANalytical B.V., the Netherlands). First, the air-dried sample were heated at 80°C for 24 h, and then ground and passed through a 200-mesh screen. The sample was placed around and at the base by boric acid, and then compressed under 30t high pressure to produce a specimen with an external diameter of 32 mm, and then placed in a desiccator before measurement. Based on the national standard GB/T14506.28-93 (silicate rock chemical analysis by X-ray fluorescence spectrometry), the optimal test conditions for each element were determined. The standard deviation and relative error were both <5%. Among the major elements, Ca, Na, Mg, and K are easily migrated elements and are easily leached during the weathering process, and their low content can indicate a hot-humid climate (called soluble elements). Si is a migration element and begins to leach only in the late stage of strong weathering process, and its low content represents a more hot-humid climate. Al and Fe are difficult to migrate and only leached under strong weathering process, their high contents represent hot-humid climate environment (called inert elements). Therefore, the Al-Fe-Si coefficient and the CIA value were used as climate proxy indicators, calculated as: $(Al_2O_3 + Fe_2O_3)/SiO_2$ and $[Al_2O_3/(Al_2O_3 + CaO + Na_2O + K_2O)] \times 100$, respectively. Higher values are associated with a stronger degree of weathering process and more hot-humid climate (Nesbitt and Young, 1982). Among the trace elements, Rb and Sr are typical discrete elements. Rb is readily absorbed by clay minerals and is retained in the place due to its large ionic radius; Sr has a smaller ionic radius and is more easily leached with water in the form of free Sr. Therefore, in the Chinese Loess Plateau, the Rb/Sr ratio is used as an indicator of precipitation and EASM intensity. The higher the Rb/Sr ratio is, the stronger the EASM intensity and precipitation are (Chen et al., 1999).

3.4 Heavy mineral analysis

For heavy mineral analysis, 1 lacustrine, 1 silty paleosol, 1 sandy paleosol, and 2 dune sand samples were selected. The separated heavy minerals were identified using a random selection of 10 views under a stereoscopic microscope using the strip method, and the results were averaged to reduce errors. Counts of more than 600 particles in each sample were used to calculate the percentage of each heavy mineral species. The results were confirmed via an internal inspection, according to the laboratory management standard of the Ministry of Land and Resources (DZ/T0130.9-2006).

The heavy minerals were separated into the following categories according to stability differences: unstable (e.g., hornblende, pyroxene), relatively stable (e.g., epidote, tremolite, garnet), stable (e.g., magnetite,

hematite, limonite, ilmenite, white titanium, sphene, kyanite, pyrite, magnesite, barite), and extremely stable minerals (e.g., monazite, rutile, zircon, tourmaline, anatase). During the weathering process, unstable and relatively stable heavy minerals are first weathered and decomposed, resulting in lower content, and extremely stable and stable heavy minerals resulting in higher content. Thus, the weathering coefficient can be used to reflect the weathering degree, such as HW index and ZTR index, calculated as: [(unstable minerals (%) + relatively stable minerals (%)) / (stable minerals (%) + extremely stable minerals (%))] and [zircon (%) + tourmaline (%) + rutile (%)], respectively. A lower HW index and a higher ZTR index are associated with a higher weathering intensity (Li et al., 1991; Shen, 1985).

4 Results

4.1 Chronology results

The AMS ^{14}C and OSL dating results are listed in Table 2 and Table 3, respectively. The age-depth relationship reveals a strong linear relationship (R = 0.996, Fig. 2). The age at the base of stratum LK19 is 78.9 ka, almost close to the orbitally-tuned age of 71 ka for the MIS5/MIS4 boundary, and the age at the top of stratum LK7 is 13.1 ka, which is close to the orbitally-tuned age of 14 ka for MIS2/MIS1 boundary (Lisiecki and Raymo, 2005). The results indicate that strata LK7-LK19 were deposited during the Last Glacial Period. In this paper, 9 chronological results are used to represent the start and end ages of main strata and their duration, then the sedimentation rate (SR) is calculated by their duration and thickness. Thereafter, we infer the start and end ages of each stratum based on different SR and adjacent known-ages (Fig. 2).

Based on the combination characteristics of sedimentary facies and their chronological ages, and comparison with the deep-sea oxygen isotope record, the Last Glacial Period of LKS was divided into five sub-stages: LKS4 (78.9−59.5 ka), LKS3c (59.5−50.5 ka), LKS3b (50.5−39.6 ka), LKS3a (39.6−29.7 ka, and LKS2 (29.7−13.1 ka), which correspond to MIS4, MIS3c, MIS3b, MIS3a, and MIS2, respectively (Lisiecki and Raymo, 2005). The ages and the stratigraphy are illustrated in Fig. 2. The time boundaries of each stage show that there is a certain age difference between the LKS and MIS. However, the dating error of LKS is between 0.9 ka and 3.8 ka; considering these dating errors, we consider that each stage in the chronological framework is comparable to the MIS framework.

4.2 Grain-size results

Sand is the most abundant grain-size fraction, with the content distribution range of 28%−91% (average 68%), followed by silt sand (7%−53%, average 25%), and clay (2%−21%, average 7%). Mz has the range of 1.76Φ−5.20Φ (average 3.08Φ) (medium sand-coarse silty sand), and the range of the SC/D ratio is 0.10−2.55 (average 0.57). There are substantial differences in the grain size composition of different sedimentary facies, as described in Table 4.

Standard deviation analysis was conducted to identify the most climatically sensitive grain size fractions among 101 particle grades in all samples. The results were used to produce a grain size-standard deviation coordinate diagram (Fig. 3(a)), with two obvious peaks ranging from 1.49Φ to 1.67Φ (315−356 μm) and 4.98Φ−5.15Φ (28−32 μm). Based on the physics of aeolian sand transport (Pye and Tsoar, 1990), the 315−356 μm fraction is the saltation component, which is associated with sediment

Table 2 The AMS ^{14}C dating results for the LKS

Stratum	Sample type	Depth/cm	Test number	^{14}C age/(a B.P.)	Calibrated a B.P.
Base of LK6	Sediment	2.42	GZ4205	11190 ± 60	13074 ± 192

Table 3 The OSL dating results for the LKS

Laboratory No.	Depth	U/ppm	Th/ppm	K/%	Equivalent dose E.D (Gy)	Annual dose Dy (Gy/Ka)	Water content/%	Age/ka
10G-610	2.78	1.81	9.06	2.20	71.27 ± 1.92	3.69	11.79	19.3 ± 0.9
18G-43	3.16	1.96	8.17	2.10	108.51 ± 5.23	3.65 ± 0.15	8.6	29.7 ± 1.9
10G-611	3.36	2.07	8.39	2.02	140.16 ± 2.30	3.57	9.55	31.9 ± 1.7
18G-44	4.11	1.80	6.32	2.33	161.55 ± 6.84	3.66 ± 0.15	6.6	44.1 ± 2.6
10G-612	4.68	2.00	7.70	2.40	191.27 ± 5.44	3.79	11.55	50.5 ± 2.5
18G-45	5.05	0.99	3.31	2.18	171.52 ± 2.74	2.88 ± 0.12	9.4	59.5 ± 2.7
10G-632	5.18	1.97	8.64	2.38	245.33 ± 9.35	3.82	12.91	64.2 ± 3.5
10G-613	5.90	1.86	7.42	2.36	291.14 ± 7.58	3.69	10.97	78.9 ± 3.8

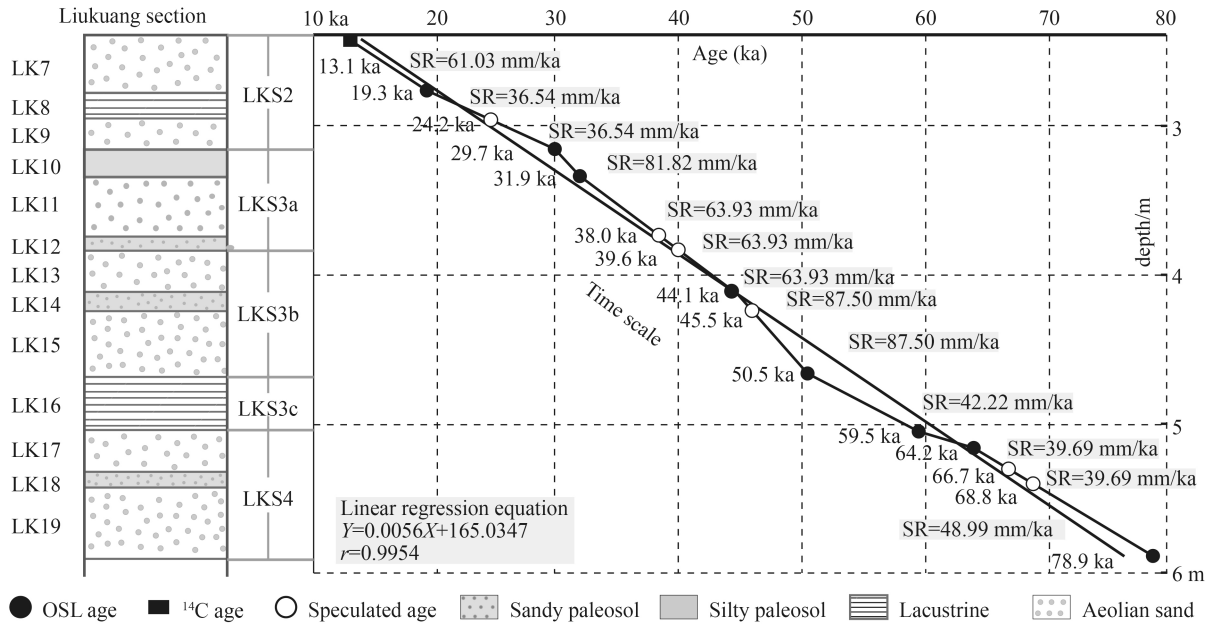

Fig. 2 Stratigraphy and age versus depth relationship for the Last Glacial in the LKS.

Table 4 Range and average of various grain-size parameters for the sedimentary facies in the LKS

	Dune sand	Sandy paleosol	Lacustrine	Silty paleosol	Whole profile
Extremely coarse sand/%	0−1.95 (0.09)	0	0−0.34 (0.05)	0−0.22 (0.04)	0−1.95 (0.09)
Coarse sand/%	5.65−32.54 (14.20)	9.82−21.69 (14.50)	8.04−11.43 (9.78)	4.56−12.16 (7.60)	4.56−32.54 (13.45)
Medium sand/%	18.46−57.92 (40.38)	31.31−53.26 (41.81)	18.38−32.89 (25.14)	10.51−19.84 (14.51)	10.51− 57.9 2(37.18)
Fine sand/%	4.84−33.46 (14.20)	6.21−19.63 (10.57)	7.96−14.83 (10.20)	3.46−7.12 (5.17)	3.46−33.46 (12.78)
Extremely fine sand/%	0.40−9.67 (3.46)	1.49−4.43 (2.86)	2.10−9.87 (5.56)	5.34−8.87 (6.97)	0.40−9.87 (3.87)
Coarse silt/%	5.37−39.10 (17.76)	10.28−30.08 (19.13)	22.58−38.25 (31.62)	29.44−42.03 (37.11)	5.37−42.03 (20.83)
Fine silt/%	1.74−7.48 (3.87)	2.10−6.77 (4.36)	5.17−8.58 (6.70)	8.81−11.72 (10.66)	1.74−11.72 (4.72)
Clay/%	1.93−14.27 (6.03)	3.10−13.37 (6.78)	8.05−14.73 (10.95)	15.61−20.69 (17.94)	1.93−20.69% (7.26%)
Mz(Φ)	1.46−4.25 (2.82)	2.21−3.56 (2.92)	3.41−4.38 (4.01)	4.46−5.20 (4.91)	1.76−5.20Φ (3.08)
SC/D	0.00−1.15 (0.42)	0.19−0.85 (0.46)	0.72−1.34 (0.98)	1.17−2.55 (1.98)	0.10−2.55 (0.57)
Coarse fraction/%	3.36−11.58 (7.65)	5.93−9.94 (7.90)	3.38−6.34 (4.71)	1.92−3.56 (2.62)	1.92−11.58 (7.03)
Fine fraction/%	0.42−3.64 (1.52)	0.83−2.50 (1.59)	1.74−3.41 (2.69)	2.36−3.36 (2.96)	0.42−3.64 (1.72)

movement under strong dynamic conditions; and the 28−32 μm fraction is the short-distance suspension component, which is associated with sediments movement under weak dynamic conditions. The proportions of the two fractions, namely coarse and fine fraction, respectively, are significantly negatively correlated (r = −0.901) (Fig. 3(b)), which indicates that they represent two different sedimentary environments (Boulay et al., 2003).

The climate of Eastern China is characterized by the alternation of the EASM and EAWM. During the prevailing periods of EAWM, the climate is cold and dry with strong winds, and aeolian sand deposition is intensified. However, when the EASM prevails, the climate is warm and humid with weak winds, and aeolian sand activity weakens or ceases (An et al., 1991). According to the chronological framework and the grain size results, the peaks of coarse fraction mainly occurs in dune sand layers while low values in paleosol layers; and peaks of fine fraction mainly occur in paleosol layers while low values in dune sand layers. Therefore, the coarse and fine fractions are regarded as proxy indicators of the EAWM and EASM intensity, respectively. The content distribution range and average in the section are 1.9%−11.6% (average 7.0%) and 0.4%−3.6% (average 1.8%), respectively.

4.3 Geochemistry results

SiO_2 is the most abundant element with the content distribution range of 67.4%−94.0% (average 83.3%), followed by Al_2O_3 (6.2%−15.5%, average 9.0%), TFe_2O_3

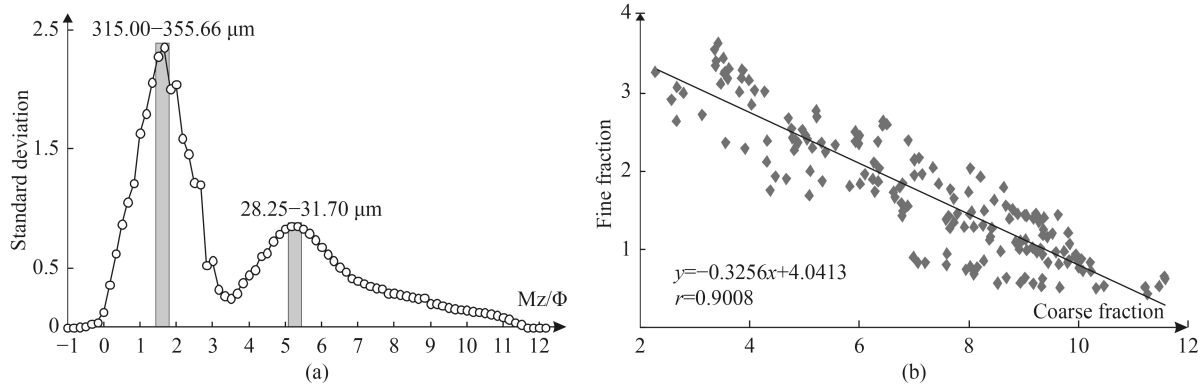

Fig. 3 (a) Grain size versus standard deviation curve of the LKS during the Last Glacial Period; (b) relationship between the coarse fraction (315−356 μm) and fine fraction (28−32 μm).

(0.6%−4.2%, average 1.8%), K_2O (2.4%−2.9%, average 2.6%), Na_2O (0.5%−1.1%, average 0.8%), MgO (0.1%−1.3%, average 0.4%), CaO (0.2%−0.5%, average 0.3%), Rb (65.6−101.9 ppm, average 78.6 ppm) and Sr (116.7−160.9 ppm, average 128.8 ppm). The CIA has the range of 55.1−75.6 (average 63.7), the Al-Fe-Si coefficient is 0.04−0.16 (average 0.07), and the Rb/Sr ratio is 0.46−0.85 (average 0.61). The chemical element compositions of different sedimentary facies are listed in Table 5.

4.4 Heavy mineral results

The heavy mineral composition is dominated by relatively stable and stable minerals, with the content distribution range of 51.5%−62.0% (average 57.3%) and 18.0%−30.5% (average 24.7%), respectively. The proportions of extremely stable and unstable minerals are substantially lower, with ranges of 7.3%−10.3% (average 8.8%) and 1.2%−3.0% (average 1.7%), respectively. The percentages of each heavy mineral, HW index and ZTR index are listed in Table 6. The HW index is the lowest in silty paleosol, followed in increasing order by lacustrine, sandy paleosol, and dune sand. The ZTR index is the highest in lacustrine, followed in descending order by silty paleosol, sandy paleosol, and dune sand.

5 Sedimentary environment analysis

5.1 Climatic environment and EAWM intensity indicated by sedimentary facies

The LKS is located in the seaward extension of the Shandong Peninsula, The LKS facing the North Yellow Sea, about 100 m away from the current coastline, and was significantly affected by sea-level fluctuations. During the Last Glacial Period, various sedimentary facies, such as dune sand, sandy paleosol, silty paleosol and lacustrine with high sand content developed, which formed several interbedding sedimentary cycles of paleosols and dune sands. To explore the climatic changes during the Last Glacial Period, it is necessary to first clarify the environmental significance of each sedimentary facies.

Among the above climate indicators, there is a clear

Table 5 The element contents of the sedimentary facies in the LKS

	Dune sand	Sandy paleosol	Lacustrine	Silty paleosol	Whole profile
SiO_2/%	73.75−94.02 (84.91)	82.74−88.60 (85.65)	72.32−82.30 (76.81)	67.37−71.58 (69.48)	67.37−94.02 (83.32)
Al_2O_3/%	6.16−12.84% (8.43)	6.31−10.00 (8.02)	9.73−13.10 (11.57)	13.59−15.52 (14.55)	6.16−15.52 (9.04)
TFe_2O_3/%	0.64−3.04% (1.55)	1.02−1.86 (1.37)	2.18−3.30 (2.74)	3.78−4.20 (3.99)	0.64−4.20 (1.78)
K_2O/%	2.38−2.87% (2.63)	2.38−2.75 (2.58)	2.56−2.86 (2.69)	2.63−2.69 (2.65)	2.38−2.87 (2.63)
Na_2O/%	0.52−1.08% (0.76)	0.52−0.78 (0.68)	0.79−0.89 (0.83)	0.77−0.82 (0.79)	0.52−1.08 (0.76)
MgO/%	0.13−0.69% (0.34)	0.23−0.56 (0.36)	0.51−0.81 (0.70)	0.93−1.26 (1.09)	0.13−1.26 (0.42)
CaO/%	0.21−0.51% (0.33)	0.23−0.35 (0.29)	0.32−0.37 (0.34)	0.34−0.3 6 (0.35)	0.21−0.51 (0.33)
Rb/ppm	65.63−88.33 (75.72)	68.11−87.32 (76.42)	84.02−90.44 (88.68)	99.25−101.9 (100.58)	65.63−101.9 (78.58)
Sr/ppm	116.98−160.91 (130.98)	116.67−137.02 (123.91)	121.22−132.06 (125.63)	119.57−125.79 (122.68)	116.67−160.91 (128.81)
CIA	55.08−70.67 (62.33)	61.04−66.06 (62.83)	64.70−71.47 (68.62)	72.43−75.59 (74.01)	55.08−75.59 (63.72)
Al-Fe-Si coefficient	0.04−0.12 (0.07)	0.05−0.08 (0.06)	0.08−0.12 (0.10)	0.13−0.16 (0.15)	0.04−0.16 (0.07)
Rb/Sr ratio	0.46−0.71 (0.58)	0.55−0.71 (0.62)	0.64−0.75 (0.71)	0.79−0.85 (0.82)	0.46−0.85 (0.61)

Table 6 Percentages of each heavy minerals, HW and ZTR index in the LKS

		Lacustrine	Silty paleosol	Sandy paleosol	Aeolian sand	
		LK8-3	LK10-5	LK14-3	LK11-11	LK17-5
Unstable minerals	Pyroxene	0.5	1	0.2	2	1
	Hornblende	1	0.8	1	1	0.2
	Tremolite	1	0.5	1	1	2
Relatively stable minerals	Epidote	43	39	52	51	57
	Garnet	12	12	6	6	3
	Magnetite	–	–	1	1	–
	Hematite	0.5	–	–	0.2	–
	Limonite	1	3	2	1	2
	Ilmenite	21	26	20	21	12
Stable minerals	White titanium	2	1	4	1	3
	Sphene	0.5	0.5	0.2	0.2	1
	Kyanite	–	–	0.2	–	–
	Pyrite	–	–	–	–	–
	Barite	0.2	–	–	–	–
	Magnesite	–	–	0.2	–	–
	Monazite	–	–	–	–	–
Extremely stable minerals	Rutile	4	2	2	0.4	1.1
	Zircon	4	4	3	3	3
	Tourmaline	2	3	3	4	4
	Anatase	0.3	0.2	0.2	0.2	0.5
Others	Others	7	7	7	7	10
HW index		1.62	1.34	1.68	1.90	2.38
ZTR index		10	9	8	7.4	8.1

Note: "–" only a few grains were observed.

internal logical relationship during the weathering process. In the warm-humid environment and EASM prevailing period, the MZ value and SC/D ratio increase due to the weak carrying capacity of the wind. At the same time, the weathering-leaching is strengthened, which leads to the leaching of soluble elements and the enrichment of inert elements, and the decomposition of unstable and relatively stable heavy minerals and the enrichment of extremely stable and stable heavy minerals. These processes lead to the increase of clay content, CIA value, Al-Fe-Si coefficient, ZTR index, and decrease of HW index and coarse fraction content. In a dry-cold environment and EAWM prevailing period, the changes in these indicators are reversed. Tables 4−6 indicate that the climate indicators such as Mz, SC/D ratio, clay content, fine fraction content, Al-Fe-Si coefficient, CIA value, Rb/Sr ratio, and ZTR index have similar variations in the sedimentary facies: The lowest values occur in dune sand, followed in increasing order by sandy paleosol, lacustrine, and silty paleosol. In contrast, the coarse fraction contents and HW index are highest in dune sand, followed in decreasing order by sandy paleosol, lacustrine, and silty paleosol.

The dune sand contains the lowest clay content, Al-Fe-Si coefficient, CIA, and ZTR indexes, but with the highest HW index and coarse fraction content. This indicates the sediment has a high degree of self-organization, which implies that the sediment remains in a natural state, and is rarely disturbed by the external environment, such as weathering, leaching, and pedogenesis. Its high degree reflects a cold-dry climate. Mz has the range of 1.46Φ−4.25Φ (average 2.82Φ), belonging to a very fine sand-medium sand grade, and the SC/D ratio has the range of 0.00−1.15 (average 0.42), and the coarse fraction content was at a maximum but the fine fraction content at a minimum. These characteristics indicate a strong EAWM (weak EASM) and aeolian sand activity. Therefore, we conclude that the dune sand is aeolian sand deposition resulting from a dry-cold climate with strong EAWM.

In sandy paleosol, the values of climate indicators are close to those of dune sand. In contrast, sandy paleosol have slightly higher clay content, Al-Fe-Si coefficient, CIA, ZTR indexes, and slightly lower of HW index and coarse fraction content. This indicates a weaker degree of self-organization, enhanced weathering and warm-humid

climate. Mz has the range of 2.2Φ−3.6Φ (average 2.9Φ), belonging to an extremely fine sand-fine sand grade; and the SC/D ratio is increased with the range of 0.19−0.85 (average 0.46), and the coarse fraction content reduced and fine fraction content increased. These characteristics indicate that the sand activity were very strong. However, compared with the dune sand development period, during the sandy paleosol development period, the EAWM weakened, and the EASM strengthened, the weathering increased, and the climate turns warmer and moister.

In lacustrine sediments, the values of clay content, Al-Fe-Si coefficient, CIA, and ZTR indexes are significantly higher than those of sandy paleosol, but the HW index and coarse fraction content are significantly lower. This indicates a further decrease of self-organization degree, enhanced weathering effect, and increased degree of warm-humid climate. Mz has the range of 3.4Φ−4.4Φ (average 4.0Φ), belonging to the ultrafine sand-coarse silty sand grade; The SC/D value increased to the range of 0.72−1.34 (average 0.98); and the coarse fraction content is significantly reduced while the fine fraction content is significantly increasing. These characteristics indicate a much stronger EASM and further weakened EAWM, and the aeolian sand activity was weakened or even interrupted. Therefore, it is believed that the lacustrine facies was formed under more warm-humid climate conditions.

In silty paleosol, the values of clay content, Al-Fe-Si coefficient, CIA, ZTR indexes, fine fraction content, and Rb/Sr ratio are the highest among all sedimentary facies, but the HW index and coarse fraction content are the lowest. These characteristics indicate the minimal degree of self-organization, enhanced weathering and more warm-humid climate. Mz has the range of 4.5Φ−5.2Φ (average 4.9Φ), belonging to the coarse silt-fine silty sand grade; The SC/D ratio has the range of 1.17−2.55 (average 1.98) dominated by silt and clay; the coarse fraction content is least and fine fraction content reaches maximum. This indicates that the EASM was very strong while the EAWM was weakening, precipitation was abundant, and sand activity was interrupted. The silty paleosol reflects the highest degree of warm-humid climatic environment.

According to the above analysis, the warm-humid degree and EASM strength reflected by the sedimentary facies is dune sand < sandy paleosol < lacustrine < silty paleosol, while the degree of dry-cold climate and EAWM strength are indicated by different sedimentary facies in dune sand > sandy paleosol > lacustrine > silty paleosol.

5.2 Climate fluctuation and monsoon evolution on ten-thousand-year timescale

The beginning and ending times of the Last Glacial Period in the LKS are 78.9 ka and 13.1ka, lasting for 65.8ka. Within the stratigraphical sequence, there are 6.5 sedimentary cycles composed of paleosol and dune sand, and the climatic indicators display corresponding peak-valley alternations, reflecting climatic and environmental changes on a ten-thousand-year timescale. The range and average values of the indicators in the major climate stages and sub-stages are listed in Table 7, and the inferred aeolian-sand activity and monsoon evolution are described next.

The LKS4, with the geological age of 78.9−59.5 ka and corresponding to the MIS4 sub-stage, is composed of two layers of dune sand (strata LK17, LK19) and a thin layer of sandy paleosol (stratum LK18). The average values of Mz, fine fraction content, SC/D ratio, CIA, and Rb/Sr ratio are the lowest during the Last Glacial Period, clay content and Al-Fe-Si coefficient are the second lowest, all of which show low valleys on the climate change curve. The coarse fraction is the second highest value in the whole interval, displaying a significant peak (Table 7 and Fig. 4). The average Mz value is 2.26Φ and the SC/D

Table 7 Average and range of climate indicators in the LKS during defined intervals of the Last Glacial Period

	Mz (Φ)	SC/D	<5 μm	Coarse fraction	Fine fraction	Al-Fe-Si coefficient	CIA value	Rb/Sr ratio
LKS2 (29.7−13.1 ka)	3.70	0.86	9.19	4.31	2.71	0.100	68.43	0.66
	2.96−4.38	0.51−1.34	6.25−14.27	3.36−5.83	1.68−3.64	0.074−0.124	64.40−71.47	0.60−0.73
LKS3a (39.6−29.7 ka)	3.43	0.85	9.18	6.62	2.11	0.088	66.38	0.68
	2.67−5.20	0.31−2.55	4.52−20.69	1.92−9.37	1.39−3.36	0.056−0.159	60.66−75.59	0.59−0.85
LKS3b (50.5−39.6 ka)	2.42	0.20	4.05	9.06	1.04	0.050	60.89	0.57
	1.46−3.30	0.00−0.56	2.48−9.32	6.79−10.21	0.63−1.84	0.045−0.058	59.14−62.95	0.54−0.59
LKS3c (59.5−50.5 ka)	3.34	0.63	9.21	5.94	1.81	0.071	63.54	0.64
	2.65−4.35	0.26−1.06	4.99−14.73	4.81−7.15	0.99−2.77	0.054−0.098	59.90−68.29	0.55−0.75
LKS4 (78.9−59.5 ka)	2.26	0.18	4.07	8.62	0.66	0.054	59.31	0.48
	1.76−3.01	0.10−0.28	1.93−6.85	6.62−11.58	0.42−0.90	0.041−0.083	55.08−60.22	0.46−0.49
Last Glacial period (78.9−13.1 ka)	3.07	0.57	7.26	7.13	1.72	0.076	64.07	0.61
	1.46−5.20	0.10−2.55	1.93−20.69	1.92−11.58	0.42−3.64	0.041−0.159	55.08−75.59	0.46−0.85

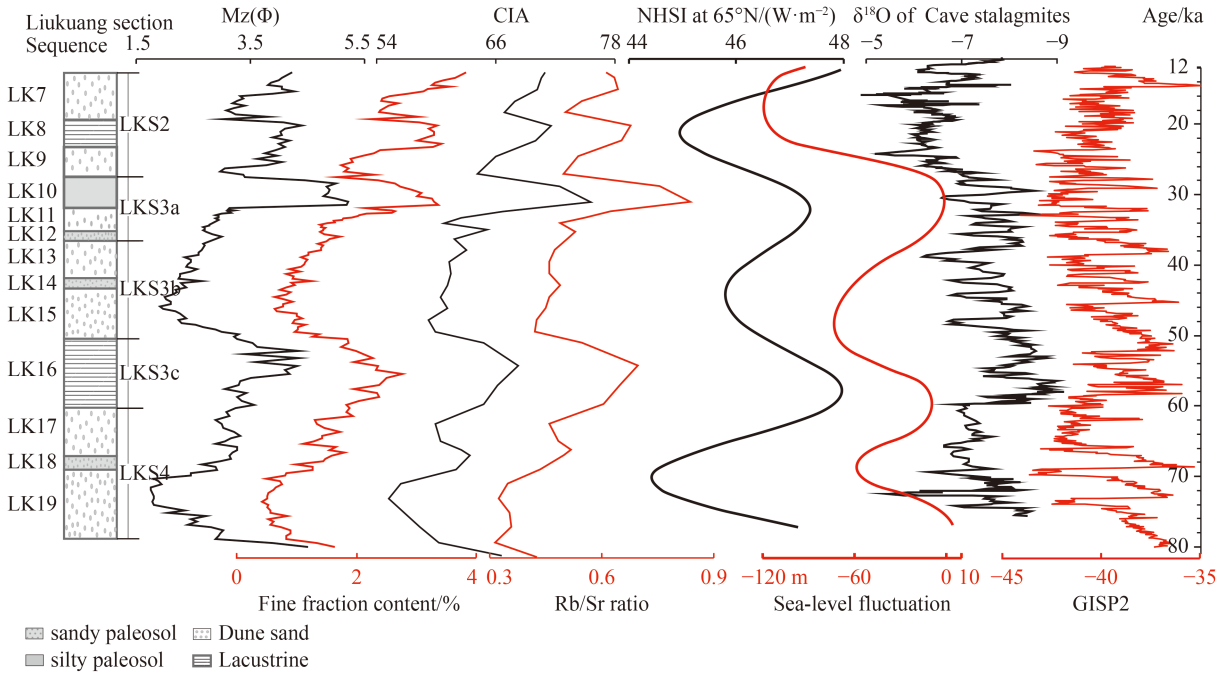

Fig. 4 Comparison of climate indicators for the LKS (Mz, fine fraction content, CIA value and Rb/Sr ratio,) with NHSI (Northern Hemisphere summer insolation, 21 July) at 65°N (Berger, 1978), sea-level fluctuations in the Yellow-Bohai Sea (IOCAS, 1985), the $\delta^{18}O$ record from cave stalagmites in subtropical China (Wang et al., 2008), and Oxygen istope in GISP2 (Stuiver and Grootes, 2000).

ratio is about 0.18, indicating it is dominated by sandy sediments, with strong wind and strong aeolian-sand activity. The content of clay and fine fraction is very low, indicating a low degree of weathering and leaching. These lead to the weak leaching degree and high content of soluble elements such as K, Ca, and Na, and low enrichment of inert elements such as Al and Fe, and then resulting in the lowest CIA value and Al-Fe-Si coefficient. These indicators generally reflect the cold-dry-windy depositional environment and the lowest degree of weathering-leaching. During the MIS4 stage, other climate indicators also indicate similar climatic conditions. In the CLP, which is to the west of the study area, it was a period with a strong winter monsoon (Porter and An, 1995) and the dust flux was generally high with the distribution range of 15−30 g/cm^2/ka (An et al., 1991). The oxygen isotope of cave stalagmite in subtropical China shows a weakening of summer monsoon (Wang et al., 2008). The Yellow-Bohai is to the north of the study area; it corresponds to the period of sea-level decline, resulting in large-scale exposure of continental shelf (IOCAS, 1985). On the orbital timescale, this phase corresponds to the low valley of Northern Hemisphere summer insolation on 21 July (NHSI) at 65°N (Berger, 1978). It suggests that the LKS4 has good consistency with the NHSI at 65°N and the climate events recorded by the surrounding carriers, with strong EAWM and weak EASM.

The LKS3c, with a geological age of 59.5−50.5 ka and corresponding to the MIS3c sub-stage, is composed of sandy paleosol and lacustrine sediments (stratum LK16). The average values of Mz, fine fraction content, SC/D ratio, clay content, Al-Fe-Si coefficient, CIA, and Rb/Sr ratio exceed those of the whole interval, showing peaks on the climate change curve. In addition, the coarse fraction content is lower than the average value, showing a low valley on the curve (Table 7 and Fig. 4). The average values of Mz and SC/D are 3.34Φ and 0.63, respectively, revealing relatively high sand content and certain intensity of aeolian sand activity, but it is obviously weaker than the LKS4 stage. The content of clay and fine fraction increased significantly, indicating enhanced weathering and leaching. As a result, the leaching degree of soluble elements increases, the content decreases, and the enrichment degree of inert elements increases, resulting in an increase of CIA value and Al-Fe-Si coefficient. It indicates that the climate during this stage became warm and humid and the weathering-leaching degree increased. During the MIS3c period, it shows a weakening winter monsoon period in the CLP (Porter and An, 1995), and the dust flux is greatly reduced, about 10−15 g/cm^2/ka (An et al., 1991); the oxygen isotope of subtropical stalagmites shows that it is summer monsoon intensification period (Wang et al., 2008); sea-level rises in the Yellow-Bohai Sea area, which corresponds to the Bohai Sea transgression (IOCAS, 1985); and the astronomical orbital scale corresponds to the peak of NHSI at 65°N (Berger, 1978). It shows that LKS3c has a good consistency with the climatic events recorded by NHSI at 65°N and surrounding carriers, with the EAWM weakened and EASM strengthened.

The LKS3b, with a geological age of 50.5−39.6 ka and corresponding to the MIS3b sub-stage, is composed of two layers of dune sand (stratum LK15 and LK13) and a thin layer of sandy paleosol (stratum LK14). The climate proxy values are very close to LKS4, the average values of Mz, fine fraction content, SC/D ratio, CIA, and Rb/Sr ratio are the second lowest during the interval, and clay content and Al-Fe-Si coefficient are the lowest; all of them show low valleys on the climate change curve. The coarse fraction content is the highest in the whole interval, showing a significant peak on the curve (Table 7 and Fig. 4). The average of Mz value is 2.42Φ and SC/D ratio is about 0.20, slightly higher than those of the LKS4, also indicating strong wind and aeolian-sand activity. The clay and fine fraction content is very low, as well as the lowest CIA value and Al-Fe-Si coefficient. These indicators generally reflect the cold-dry-windy depositional environment similar to LKS4, and the lowest weathering-leaching degree. The MIS3b stage was a period of strong winter monsoon in the CLP (Porter and An, 1995): the Md became coarser but the dust flux was similar to that of MIS3c (An et al., 1991); the oxygen isotope of the stalagmite in the subtropical zone shows weakening of summer monsoon (Wang et al., 2008); and the Yellow-Bohai Sea remained the period of sea-level decline, with large-scale exposure of the continental shelf (IOCAS, 1985). On the orbital timescale, this period corresponds to the low valley of NHSI at 65°N (Berger, 1978). It indicates that the LKS3b has a good consistency with the NHSI at 65°N and the climate events recorded by the surrounding carriers; the EAWM is strong and the EASM is weak.

The LKS3a, with a geological age of 39.6−29.7 ka and corresponding to the MIS3a sub-stage, is mainly composed of silty paleosol (stratum LK13), sand paleosol (stratum LK11), and dune sand (stratum LK12). The average values of Mz, fine fraction content, SC/D ratio, clay content, Al-Fe-Si coefficient, CIA, and Rb/Sr ratio exceed those of the average of whole interval, showing peaks on the curve. In addition, the coarse fraction content is lower than the average value, showing low valley in the curve (Table 7 and Fig. 4). The average value of Mz and SC/D are 3.43Φ and 0.85, respectively, and are similar to that of LKS3c, also displaying that the sand content is relatively high, and indicating certain intensity of aeolian sand activity, but it is obviously weaker than those of LKS3b and LKS4. The content of clay and fine fraction increased significantly, also with an increase of CIA value and Al-Fe-Si coefficient. These climate indexes indicate that the climate became warm and humid during this stage, and the weathering-leaching degree increased. During the MIS3a period, it shows a weakening winter monsoon period in the CLP (Porter and An, 1995), and the dust flux is greatly reduced to about 10−15 g/cm^2/ka (An et al., 1991); the oxygen isotope of subtropical stalagmites indicates that it is summer wind intensification period (Wang et al., 2008); the sea-level rises in the Yellow-Bohai Sea area and corresponds to the Xianxian transgression (IOCAS, 9185); and the astronomical orbital scale corresponds to the peak of NHSI at 65°N (Berger, 1978). These records show that LKS3c has a good consistency with the climatic events recorded by NHSI at 65°N and surrounding carriers, with the EAWM weakened and EASM strengthened.

The LKS2, with a geological age of 29.7−13.1 ka and corresponding to the MIS2 sub-stage, composed of two layers of aeolian sand (strata LK7 and LK9) and one layer of lacustrine sediment(stratum LK8). The average values of Mz, fine fraction, SC/D ratio, clay concentration, Al-Fe-Si coefficient, CIA, and Rb/Sr ratio are the highest during the whole interval, whereas the coarse fraction content is the lowest. These characteristics probably indicate that this sub-stage was the warmest period in the Last Glacial, and its weathering degree was the highest. However, to the other climate carriers of MIS2, it is an obvious cold period, such as the enhanced winter monsoon in the CLP (Porter and An, 1995) and the dust flux is generally high with the distribution range of 20−25 g/cm^2/ka (An et al., 1991). The oxygen isotope of the stalagmite in the subtropical China shows weakening of summer monsoon (Wang et al., 2008), and the Yellow-Bohai Sea corresponds to the significant decline of sea-level, 120−130 m lower than today (IOCAS, 1985). On the orbital timescale, this phase corresponds to the low valley of NHSI at 65°N (Berger, 1978). This contradictory phenomenon leads to the question whether LKS2 is in a cold or warm period.

According to the changes in stratigraphic composition and climate indicators of LKS2, we find that the average Mz of dune sand (LK7 and LK9) are finer than those of LKS3 and LKS4, but the average Mz of the lacustrine layer (LK8) is coarser than that of the silty paleosol (LK10) of LKS3a, and the CIA values and Rb/Sr ratio of LKS2 are lower than those of LKS3. It indicates that the climate was not as warm-humid as LKS3c and LKS3a. This phenomenon should relate to the changes of erosion-transport-deposition centers which resulted from the decline of sea-level. It is known that the sea-level decreased significantly during the MIS2 period, and dropped to −120 – −130 m during the peak period (Murray-Wallace and Woodroffe, 2014). This caused the coastline to move eastward several hundred kilometers, exposing the entire continental shelf of the Yellow-Bohai Sea and partial shelf of the East China Sea, leading to the integration of the study area with the Bohai Sea, the Yellow Sea, and the Korean Peninsula (IOCAS, 1985). The marine strata and paleosol formed in MIS3a were exposed and became new erosion-transport centers, and these sediments were carried downwind by the winter monsoon to form a desert-loess sedimentary system. For example, the aeolian sand deposited on the continental shelf of the Yellow and Bohai Sea (Zhao, 1995), the

"Liukuang red bed" developed on the northern coast of Shandong Peninsula (Zhang and Liu, 1992), silty paleosol developed in the Miaodao islands, located 200 km to the west of study area (Du et al., 2016), and loess sediments developed in the Buxi section in Zhangqiu County in Jinan City, 320 km to the south-west (Xu et al., 2014). Moreover, sea-level decline leads to the eastward movement of erosion-transport center, which in turn resulted the substantial increase of transport distance and a gradual weakening of transport capacity during transport process. Under the influence of sedimentation sorting, the grain size deposited in study area became finer, even during the period of increased aeolian-sand activity, such as average Mz in the dune sands in LKS2 being finer than that of LKS3 and LKS4.

According to previous studies, although the winter monsoon is strong during the MIS2 period, the intensity of the summer monsoon activity cannot be ignored, especially the coastal areas in the eastern Eurasian continent. For example, Sun et al. (1996) proposed that the north-western boundary of summer winds can reach the belt stretching of Chunhua-Yuexian-Lantian in the CLP. In addition, the LKS adjacent to the North Yellow Sea and is greatly influenced by the warm-humid air flow from the Pacific Ocean. As a result, the EASM brings precipitation which promotes weathering and pedogenesis. Thus, there is a lacustrine layer (LK8, age 19.3−24.2 ka) containing a large amount of organic matter in the LKS2, indicating that the precipitation in this stage was relatively abundant. This warm-humid climate is also clearly reflected in the surrounding records. For example, in the Buxi section, peaks in Mz occurred during 24−17 ka and valleys at 28−24 ka and 17−13 ka (Xu et al., 2014); the oxygen isotope of subtropical stalagmite also showed a clear peak in 21−19 ka of MIS2, indicating an enhanced EASM period (Wang et al., 2008); and GISP2 also showed a peak at 21−18 ka. Based on these indexes, it is believed that the phase−enhancing summer monsoon not only brought precipitation, but also strengthened weathering and pedogenesis, resulting in the development of lacustrine containing more organic matter in LK8.

In the context of cold climate and sea-level decline, there was an increase in the aeolian sand transport distance and sedimentation sorting effect, resulting in the deposition of finer sand sediments compared to MIS3b and MIS4. The previous studies believed that the MIS2 sediments in this area inherited the characteristics of the MIS3a sediments to some extent (Zhao, 1995). Coupled with the influence of post-depositional weathering and pedogenesis, the LKS2 presents a very hot-humid "artifact". According to the above analysis, we believed that the LKS2 climate environment is synchronized with the global climate during the MIS2 stage.

6 Discussion

The ten-thousand-year timescale climate fluctuations revealed by last glacial sediments in the LKS are mostly synchronized with polar ice cores (Stuiver and Grootes, 2000), deep-sea oxygen isotopes (Heinrich, 1988), cave stalagmites of southern China (Wang et al., 2008), loess in the CLP (Porter and An, 1995; An et al., 1991), sea-level fluctuation of the Yellow-Bohai Sea (IOCAS, 1985), and NHSI at 65°N (Berger, 1978) (Fig. 4). It reflects consistency with regional and global climate changes.

During the Last Glacial Period in the LKS, the average Mz is 119 μm (the distribution range is 27−363 μm), and the average SC/D is 0.57 (the range is 0.10−2.55), reflecting that the Last Glacial Period was dominated by sand. According to the principle of sand movement, sand grains of 70−500 μm move mainly in a jumping manner, and those of 20−70 μm are mainly suspended for a short period of time, which is difficult to transport to places 30 km away from the source area (Pye and Tsoar, 1990). According to the distribution range of Mz in the Last Glacial Period, the main part is considered to belong to the near-source accumulation material. Previous studies also show that the provenance of the loess in central Shandong Province and the sandy sediments in the northern coastal zone have multiple sources, but they are mainly proximal sediment source, which are transported by local winds (Cao et al., 1988; Lin et al., 2021; Wang et al., 2021.)

The LKS is located in the seaward extension of the Shandong Peninsula, facing the North Yellow Sea, and about 100 m away from the present coastline. Climate change constrains the monsoon intensity, weathering degree, and sea-level fluctuation. The monsoon intensity affects the intensity of aeolian sand activity, sea-level fluctuation affects the provenance supply of aeolian sand activities, which cause the erosion-transportation-deposition center and transport distance to change. When sea-level falls, the continental shelf and its loose sediments are exposed to the amospheric environment; when the sea-level rises, the waves erode the coastal sediment and transport the loose sediments to accumulate at downwind areas. Both cases can provide abundant opportunity for sand movement. Under the influence of the EAWM, these loose sediments were transported to the study area from north to south to form sandy deposits in LKS.

During the cold sub-stages of the Last Glacial Period (such as LKS4, LKS3b, and LKS2), due to the decrease of total solar radiation, the global temperature decreased, resulting in a decline of sea-level in the Yellow-Bohai Sea. The falling sea-level causes the coastline to move eastward, which not only expands the land area of Eurasia and increases the continental degree, but also strengthens the Mongolia-Siberia high and increases the EAWM intensity (Liu, 2009). The eastward movement of coastline makes the erosion-transportation-deposition center of ocean-land-atmosphere interaction also move eastward, the loose sediments of continental shelf are exposed

under the atmospheric environment providing sufficient provenance for sand movement and generate new aeolian sand activity centers. The strong EAWM erodes loose sediments on the continental shelf and formed sand active period, and then developed sandy sediments in downwind areas (e.g., LKS4 and LKS3b are composed of dune sand and sandy paleosol). Due to the low temperature and sparse precipitation, the weathering-leaching degree is low, and finally develops dune sands with high degree of self-organization.

During the warm sub-stages of the Last Glacial Period (LKS3c and LKS3a), due to the increase of total solar radiation, the global temperatures increased, which lead to the rise of sea-level in the Yellow-Bohai Sea. During the sea-level ascending process, waves eroded the loose sediments along the way and carried them to accumulate on the coastal area or beach to form sandy deposits, providing adequate sediment source for aeolian-sand activity. At this time, the Mongolia-Siberia high and EAWM intensity decreased, while the EASM increased, leading to the increase of precipitation and vegetation coverage, also strengthening the weathering - leaching - pedogenesis process, and then developing the lacustrine, silty paleosol, and sandy paleosol facies. Thus, the silty paleosol or sandy paleosol are predominant during the LKS3c and LKS3a, with low degree of self-organization.

As the result of above discussion, the external factor for the changes of successive sedimentary facies and climate proxy indexes on a ten-thousand-year scale is from the change of solar radiation, while the internal factor is monsoon changes and sea-level fluctuations.

7 Conclusions

Based on the study of the Last Glacial deposition and climatic proxy indexes in LKS, the characteristics of climate changes and the driving factors are as follows.

1) The dry-cold degree and EAWM intensity are reflected by each sedimentary facies are dune sand > sandy paleosol > lacustrine > silty paleosol.

2) On ten-thousand-year timescale, the EAWM strengthened during LKS4 (78.9−59.5 ka), LKS3b (50.5−39.6 ka) and LKS2 (29.7−13.1 ka), which correspond to MIS4, MIS3b, and MIS2, respectively; and the EAWM weakened during LKS3c (59.5−50.5 ka) and LKS3a (39.6−29.7 ka), which correspond to MIS3c and MIS3a, respectively.

3) The climatic events were essentially synchronous with regional and global climate changes. It suggests that the external driving factor is from the changes of solar radiation, and the internal is mainly from the combined effect of monsoon changes and sea-level fluctuations.

Acknowledgment This study was supported by the National Natural Science Foundation of China (Grant Nos. 41571007 and 41201006); the Strategic Priority Research Program of the Chinese Academy of Sciences (Category B; No. XDB26000000); the Open Fund Project of the State Key Laboratory of Nuclear Resources and Environment (No. NRE1507); Guangdong Basic and Applied Basic Research Foundation (No. 2020A1515011071); Guangdong Innovation Project (No. 2018KTSCX213).

References

An Z S, Kukla G, Porter S C, Xiao J L (1991). Late Quaternary dust flow on the Chinese Loess Plateau. Catena, 18(2): 125–132

An Z S, Porter S C (1997). Millennial-scale climatic oscillations during the last interglaciation in central China. Geology, 25(7): 603–604

An Z S, Wu G X, Li J P, Sun Y B, Liu Y M, Zhou W J, Cai Y J, Duan A M, Li L, Mao J Y, Cheng H, Shi Z G, Tan L C, Yan H, Ao H, Chang H, Feng J (2015). Globle monsoon dynamics and climate change. Annu Rev Earth Planet Sci, 43(1): 29–77

Andreucci S, Clemmensen L B, Murray A S, Pascucci V (2009). Middle to late Pleistocene coastal deposits of Alghero, northwest Sardinia (Italy): chronology and evolution. Quat Int, 07(025): 1–14

Berger A L (1978). Long-term variations of caloric insolation resulting from the Earth's orbital elements. Quat Res, 9(2): 139–167

Boulay S, Colin C, Trentesaux A, Pluquet F, Bertaux J, Blamart D, Buehring C, Wang P (2003). Mineralogy and sedimentology of Pleistocene sediment in the South China Sea (ODP Site 1144). In: Proceedings of the Ocean Drilling Program Scientific Results, 184: 1–21

Cao J X, Li P Y, Shi N (1988). Study on the loess of Miaodao Islands in Shandong Province. Sci China Ser B Chem Life Sci Earth Sci, 31(01): 120–127

Chen J, An Z S, Wang Y J, Ji J F, Chen Y, Lu H Y (1999). Distribution of Rb and Sr in the Luochuan Loess-paleosol sequence of China during the last 800 ka——implications for paleomonsoon variations. Sci China Ser D Earth Sci, 42(3): 225–232

Cheng H, Edwards R L, Sinha A, Spötl C, Yi L, Chen S J, Kelly M, Kathayat G, Wang X F, Li X L, Kong X G, Wang Y J, Ning Y F, Zhang H W (2016). The Asian monsoon over the past 640000 years and ice age terminations. Nature, 534(7609): 640–646

Ding Z L, Ren J Z, Liu D S, Sun J M, Zhou X Q (1996). The irregular millennial variations and its mechanism of monsoon-desert system during late Pleistocene. Sci China Ser D Earth Sci, 26(5): 385–391 (in Chinese)

Du S H, Li B S, Li Z W, Chen M H, Xiang R, Zhang D D, Niu D F, Zhang L L (2014). Rapid changes in the East Asian Monsoon during the Last Interglacial in the Bohai Sea coastal zone, China. J Sediment Res, 84(2): 88–96

Du S H, Li B S, Li Z W, Chen M H, Zhang D D, Xiang R, Niu D F, Si Y J (2016). East Asian monsoon precipitation and paleoclimate record since the last interglacial period in the Bohai Sea coastal zone, China. Terr Atmos Ocean Sci, 27(6): 825–836

Folk R L, Ward W C (1957). Brazos River Bar (Texas): a study in the significance of grain size parameters. J Sediment Res, 27(1): 3–26

Fornós J J, Clemmensen L B, Gómez-Pujol L, Murray A S (2009). Late Pleistocene carbonate aeolianites on Mallorca, Western Mediterranean: a luminescence chronology. Quat Sci Rev,

28(25–26): 2697–2709

Gao Y X (1962). Some Problems of East Asian Monsoon. Beijing: Science Press (in Chinese)

Guo Y S, Li D G (1994). On the geological time of Chengshantou "Liukuang Red Beds" from regional climatic stratigraphy. Marine sciences, (4): 64–65 (in Chinese)

Heinrich H (1988). Origin and consequences of cyclic ice rafting in the northeast Atlantic Ocean during the past 130000 years. Quat Res, 29(2): 142–152

IOCAS (1985). Marine geology laboratory, Institute of Oceanology, Chinese Academy of Sciences. Geology of Bohai Sea. Beijing: Science Press (in Chinese)

Konert M, Vandenberghe J (1997). Comparison of laser grain size analysis with pipette and sieve analysis: a solution for the underestimation of the clay fraction. Sedimentology, 44: 523–535

Li B S, Dong G R, Gao S Y, Ding T H, Shen J Y, Shao Y J (1991). The change in climatic environment of the Salawusu River area since the terminal stage of Mid-Pleistocene as indicated by detrital minerals in quaternary sediments. Acta Petrologica et Mineralogica, 10(1): 84−90 (in Chinese)

Li W B, Li Z W, Wang Z G, Ma Z Y, Wang Z Z, Liang L C (2019). Climatic environment changes during the last interglacial-glacial cycle in Zhifu loess section: revealed by grain-size end-member algorithm. Mar Geo Quat Geo, 39(2): 177–187 (in Chinese)

Lin X, Liu J, Wu Z H, Liu W M, Li C A, Li Z W, Wang S M, Liu H J, Chen J X (2021). Provenance of the Loess in Shandong Province (Eastern China) during the Last Ice Age: constraints from the U-Pb Age of Detrital Zircons. Earth Sci, 46(9): 3230–3244 (in Chinese)

Lisiecki L E, Raymo M E (2005). A Pliocene-Pleistocene stack of 57 globally distributed benthic $\delta^{18}O$ records. Paleoceanography, 20(PA003): 1–17

Liu T S (1985). Loess and the Environment. Beijing: Ocean Press (in Chinese)

Liu T S (2009). Loess and Arid Environment. Hefei: Anhui Science & Techonology Press (in Chinese)

Local History Compilation Committee of Rongcheng in Shandong Province (1999). Rongcheng History. Jinan: Qilu Press (in Chinese)

Murray-Wallace C V, Woodroffe C D (2014). Quaternary Sea-level Changes—A Globle Perspective. London: Cambridge University Press: 256–316

Nesbitt H W, Young G M (1982). Early Proteozoic climates and plate motions inferred from major element chemistry of lutites. Nature, 299(5885): 715–717

Porter S C, An Z S (1995). Correlations between climate events in the North Atlantic and China during the last glaciation. Nature, 375(6529): 305–308

Pye K, Tsoar H (1990). Aeolian Sand and Sand Dunes. Londan: Hyman Unwin

Shen L Q (1985). Some important conceptions and their application in the study of heavy minerals of sedimentary rocks. China Ser B Chem Life Sci Earth Sci(12): 1321–1332

Stuiver M, Grootes P M (2000). GISP2 oxygen istope ratios. Quat Res, 53(3): 277–284

Sun D H, Wu X H, Liu D S (1996). Evolution of the summer monsoon regime over the Loess Plateau of the last 150 ka. Sci China Ser D Earth Sci, 39(5): 503–511

Wang Y D, Yang S L, Ding Z L (2021). Provenance and paleoclimatic implications of loess deposits in Shandong Province, eastern China. Quat Res, 103: 88–98

Wang Y J, Cheng H, Edwards R L, An Z S, Wu J Y, Shen C C, Dorale J A (2001). A high-resolution absolute-dated late Pleistocene Monsoon record from Hulu Cave, China. Science, 294(5550): 2345–2348

Wang Y J, Cheng H, Edwards R L, Kong X G, Shao X H, Chen S T, Wu J Y, Jiang X Y, Wang X F, An Z S (2008). Millennial- and orbital-scale changes in the East Asian monsoon over the past 224000 years. Nature, 451(7182): 1090–1093

Xu S J, Ding X C, Ni Z C (2014). The sedimentary characteristics of Buxi loess profile in Shandong Province and their paleoclimatic and palaeoenvironment significance. Acta Geogr Sin, 69(11): 1707–1717 (in Chinese)

Yi L, Shi Z G, Tan L C, Deng C L (2017). Orbital-scale nonlinear response of East Asian summer monsoon to its potential driving forces in the late Quaternanry. Clim Dyn, 50(5–6): 2183–2197

Yi L, Yu H J, Ortiz J D, Xu X Y, Chen S L, Ge J Y, Hao Q Z, Yao J, Shi X F, Peng S Z (2012). Late Quaternary linkage of sedimentary records to three astronomical rhythms and the Asian monsoon, inferred from a coastal borehole in the south Bohai Sea, China. Palaeogeogr Palaeoclimatol Palaeoecol, 329–330: 101–117

Zazo C, Mercier N, Lario J, Roquero E, Goy J L, Silva P G, Cabero A, Borja F, Dabrio C J, Bardají T, Soler V, García-Blázquez A, Luque A D (2008). Palaoenvironmental evolution of the Barbate-Trafalgar coast (Cadiz) during the last 140ka: climate, sea-level interactions and tectonics. Geomorphology, 100(1–2): 212–222

Zhang M S, Liu J (1992). The sequence, division, genesis and climatic implication of "Liukuang Red Beds" in Chengshantou, Rongcheng county. Mar Geo Quat Geo, 12(1): 73–83 (in Chinese)

Zhao S L (1995). Desertification of Continental Shelf. Beijing: Science Press (in Chinese)